Uniaxial and Shear Deformations in Smectic-C Main-Chain Liquid-Crystalline Elastomers

Antoni Sánchez-Ferrer and Heino Finkelmann*

Albert-Ludwigs-Universitaet, Institut für Makromolekulare Chemie, Hermann-Staudinger-Haus, Stefan-Meier-Str. 31, 79104 Freiburg, Germany

Received August 14, 2007; Revised Manuscript Received November 27, 2007

ABSTRACT: A novel cross-linked smectic-C main-chain liquid-crystalline elastomer has been synthesized by polycondensation of vinyloxy-terminated mesogens, tetramethyldisiloxane and pentamethylpentaoxapentasilecane. The introduction of the functional vinyloxy group allows the synthesis of well-defined networks having low soluble content and good mechanical properties due to elimination of side reactions as in the case of vinyl groups. Networks having a macroscopic uniformly ordered director and a conical distribution of the smectic layer normal with respect to the director are mechanically deformed by uniaxial and shear deformations. Under uniaxial deformations two processes were observed: parallel to the director the mechanical field directly couples to the smectic tilt angle while perpendicular to the director a reorientation process takes place. A shear deformation parallel and perpendicular to the director causes a uniform layer orientation and the network exhibits a smectic-C monodomain phase having a macroscopic uniform director and layer orientation. This process is reversible for shear deformation perpendicular and irreversible by applying the shear force parallel to the director.

Introduction

Smectic elastomers, due to their layered structure, exhibit distinct anisotropic mechanical properties and mechanical deformation processes parallel or perpendicular to the smectic layer normal, causing different responses of the networks. Besides the anisotropy of the mechanical moduli, reorientation processes are of interest. The most important aspect is whether an external mechanical field parallel and perpendicular to the smectic layer normal couples either to the orientational order of the mesogenic units, the director, or to the layer orientation. Up to date only side-chain liquid-crystalline elastomers (SCLCEs) with smectic-A (SmA) and smectic-C (SmC) phases have been analyzed with respect to their anisotropic mechanical properties.

In the case of macroscopically ordered SmA SCLCEs, uniaxial mechanical deformations have been performed parallel and perpendicular to the director.[1−3] The Young's modulus parallel to the layer normal equates the smectic layer compression modulus and reflects the enthalpy elasticity along this direction of the smectic phase structure. Perpendicular to the layer normal the modulus reflects the entropy elasticity of the polymer network and typically differs by about 2 orders of magnitude. While the first deformation process causes layer reorientation above a characteristic threshold stress, the second process leaves the structure unmodified and indicates the in-plane fluidity of the smectic layers.[4,5] Very recently, networks having the SmÃ phase structure exhibit no layer reorientation under deformation parallel to the layer normal. Because here the SmÃ phase can be considered as consisting of smectic blocks separated by defects, the deformation process occurs along the defects without affecting the orientation of the blocks.[6]

SmC elastomers, significant because of their optical and ferroelectric properties such as in the case of chiral molecules (SmC* phase),[7] have also been synthesized. By applying a multistage cross-linking process, macroscopic uniformly ordered networks are now realizable. In the first stage a uniaxial deformation couples to the director orientation and causes a uniform director alignment parallel to the deformation axis while the orientation of the smectic layer normal is conically distributed about the director. A second process, either shear deformation perpendicular to the director or a uniaxial deforma-

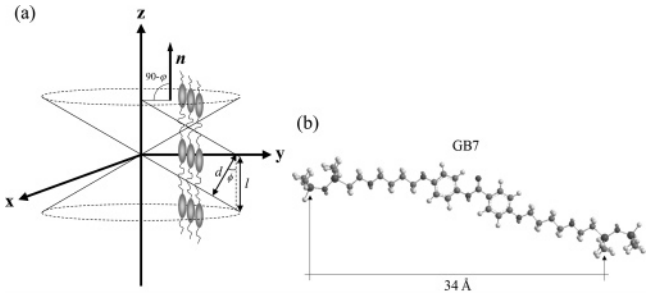

Figure 1. (a) Conical layer distribution structure of a SmC main-chain elastomer. In this picture the descriptions of the distances (d) and angles (φ, ϕ) of monomers and layers and length (l) between repeating units are shown. (b) Molecular dimensions of the monomer unit GB7.

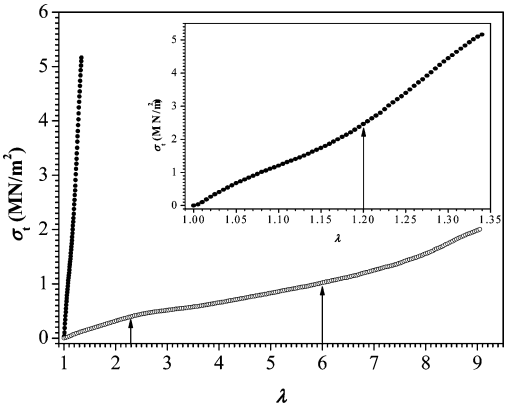

Figure 2. Uniaxial stress−strain curves parallel (●) and perpendicular (□) to the director on a conical layer distribution structure of the elastomer MCEB7Azo2-2.5 at 25 °C in the SmC phase. (σ_t = true uniaxial stress. The arrows indicate regions of changing slope; refer to text.) Inset: uniaxial stress−strain curve parallel to the director.

* Corresponding author: Tel +49 761 203 6274; Fax +49 761 203 6306; e-mail Heino.Finkelmann@makro.uni-freiburg.de.

10.1021/ma7025644 CCC: $40.75
Published on Web 01/05/2008

Scheme 1. Synthesis of SmC MCLCE (MCEB7Azo2-2.5)

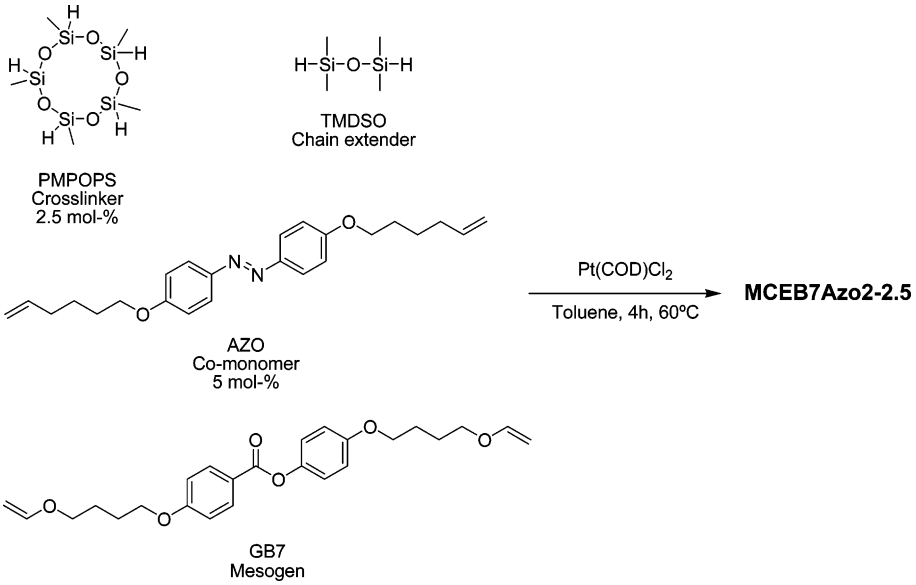

tion perpendicular to the smectic layer normal, forms a monodomain.[8−11] In recent papers[12−14] theoretical models have been developed for deformations in SmA[15−17] and SmC[18,19] liquid-crystalline elastomers.

So far experiments on the deformation of SmC SCLCEs do not indicate any changes of the tilt angle between the director and the layer orientation. The basic question is whether main-chain liquid-crystalline elastomers (MCLCEs), where the mesogenic units are directly incorporated into the polymer backbone, differ in their mechanical response.

In this paper, the mechanical response of new SmC MCLCEs will be described under uniaxial or shear deformations which are applied parallel or perpendicular to the director. The orientation and reorientation processes of the SmC elastomer are studied to identify whether the director and/or layers couple with the applied external mechanical field. The SmC elastomer is a monodomain with respect to the director orientation but has a conical orientation distribution of the layer normal with respect to the director as deduced from the X-ray patterns.

Synthesis and Characterization

Synthesis of the Mesogen and Comonomer. For the synthesis of the SmC MCLCE, the well-known one-pot hydrosilylation polyaddition reaction of a bifunctional mesogenic

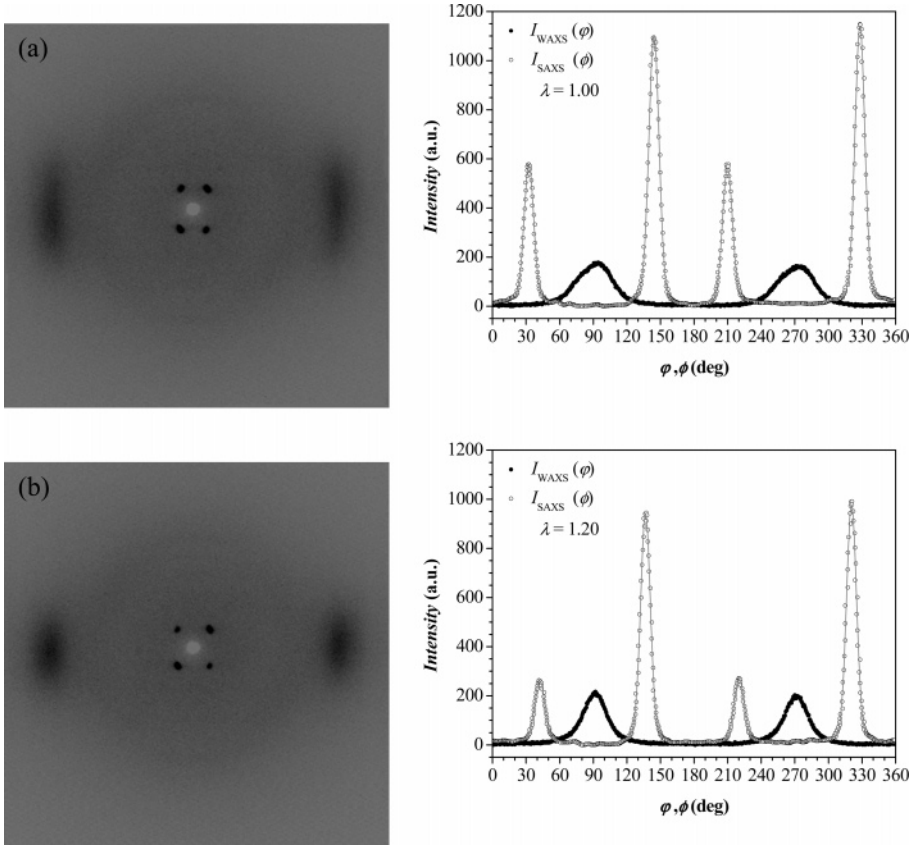

Figure 3. X-ray pictures of the MCEB7Azo2-2.5 sample at 25 °C in the SmC phase and WAXS and SAXS azimuthal intensity distributions at the uniaxial strain parallel to the director of (a) $\lambda = 1.00$ and (b) $\lambda = 1.20$.

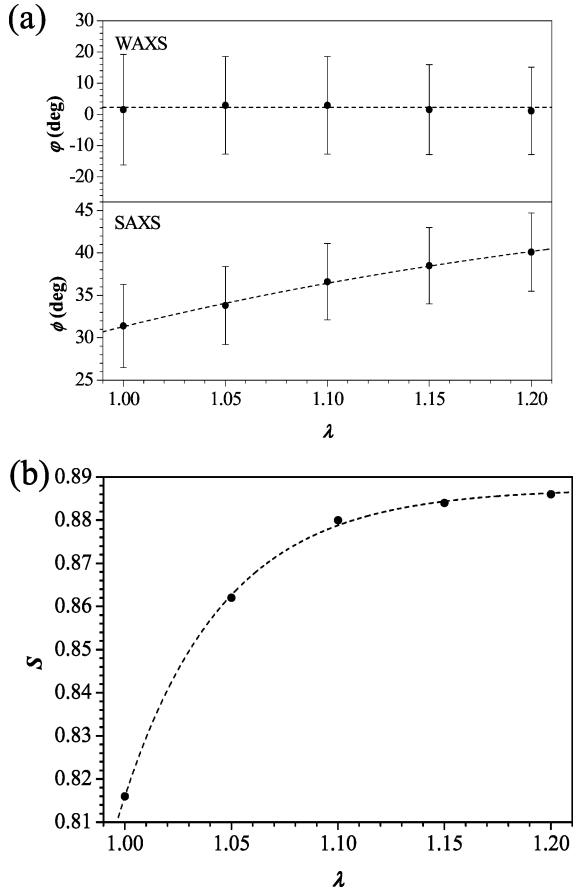

Figure 4. (a) Peak maxima in the WAXS (φ) and SAXS (ϕ) azimuthal intensity distributions as a function of uniaxial strain parallel to the director, λ. (b) Order parameter, S, as a function of uniaxial strain parallel to the director, λ.

monomer containing two terminal vinyl groups with tetramethydisiloxane (TMDSO) and the pentafunctional cross-linker (PMPOPS) as developed by Donnio was applied.[20] The main problems of this procedure, however, are the purity of the precursor olefins used for the synthesis of the monomers and the side reactions of the hydrosilylation such as isomerization and migration of the olefinic double bond. These problems cause a considerable amount of soluble byproducts that are isolated when extracting the network. To overcome these problems, high-purity (>99%) commercially available functional vinyl ether compounds are employed for the synthesis of the monomer. Furthermore, the vinyloxy group prevents any parallel reaction during the hydrosilylation addition due to the ether group. Because the vinyl ether chains are highly sensitive to small quantities of water, they have to be introduced in the final step of the synthesis. The mesogenic core, 4-hydroxyphenyl 4-hydroxybenzoate, HPHB, is synthesized by esterification of 4-hydroxybenzoic acid with hydroquinone,[21] and finally the vinyloxy chain, 4-(vinyloxy)butan-1-ol, was attached via a Mitsunobu reaction[22] to obtain the mesogenic monomer GB7 (Scheme 1). The azobenzene derivative, AZO, was introduced as a comonomer because of further photoisomerization studies in this photoactive sample. The (*E*)-4-hydroxy-4′-methoxyazobenzene, MHAB, was synthesized according to the literature[23−25] and the (*E*)-4,4′-dihydroxyazobenzene, DHAB, by demethylation of MHAB.[26] The comonomer (*E*)-4,4′-bis(hex-5-en-1-yloxy)azobenzene (AZO) was synthesized via alkylation of the phenolic groups[27] on introducing two olefinic chains on both sides of the aromatic core of DHAB.

Synthesis and Characterization of the Network. The smectic-C main-chain liquid-crystalline elastomer (MCEB7Azo2-2.5) was prepared using the spin-casting technique, as shown in Scheme 1. A concentration of 2.5 mol % of the isotropic cross-linker, 2,4,6,8,10-pentamethyl-1,3,5,7,9,2,4,6,8,10-pentaoxapentasilecane (PMPOPS), was applied which corresponds to a 6.25 mol % of the total amount of reactive hydrogen. After the noncomplete hydrosilylation reaction, the sample was removed from the reactor and aligned by applying a uniaxial stress. For the completion of the hydrosilylation reaction, the network was cured under load during the second step of the cross-linking reaction in order to align and fix the liquid crystal phase.

The elastomer was characterized by standard methods. With respect to the director alignment X-ray measurements reveal a well-oriented sample having an order parameter of $S = 0.78 \pm 0.02$ at 25 °C. The soluble content extracted with hexane is 5.7%. From the DSC measurements the phase transition temperatures and transformation enthalpies are determined to be g −1 °C (0.2 J g^{-1} K^{-1}) SmH 12 °C (4 J g^{-1}) SmC 51 °C (8 J g^{-1}) I. Swelling experiments in toluene at 25 °C confirm a low cross-linking density with the swelling factor of $q = 15.4 \pm 0.4$. The swelling anisotropy is $q_z = \alpha_x/\alpha_z = 8.2 \pm 0.2$, where z is the stress axis during the second cross-linking reaction, which also corresponds to orientation of the director, and where α_z and α_x are the swelling ratios in the parallel and perpendicular direction to the director. The sample exhibits a conical layer distribution structure as schematically presented in Figure 1a. The mesogens are oriented in the z-direction, and the layers are distributed conically about z. This structure is elucidated from the X-ray experiment (Figure 3a) and yields the mesogen distance of 4.5 Å, layer distance $d = 25$ Å, and layer angle $\phi = 30°$. The calculated length of the monomer unit is $l = 29$ Å, which is close to the all-trans length of 34 Å, as given in Figure 1b.

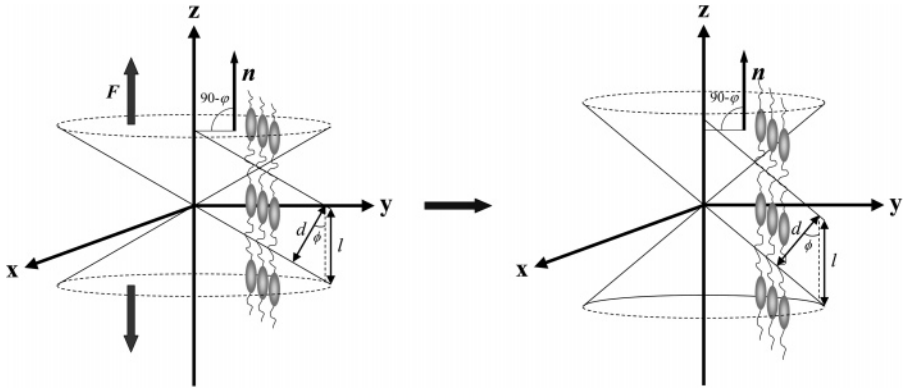

Figure 5. Uniaxial deformation process parallel to the director on a SmC MCLCE.

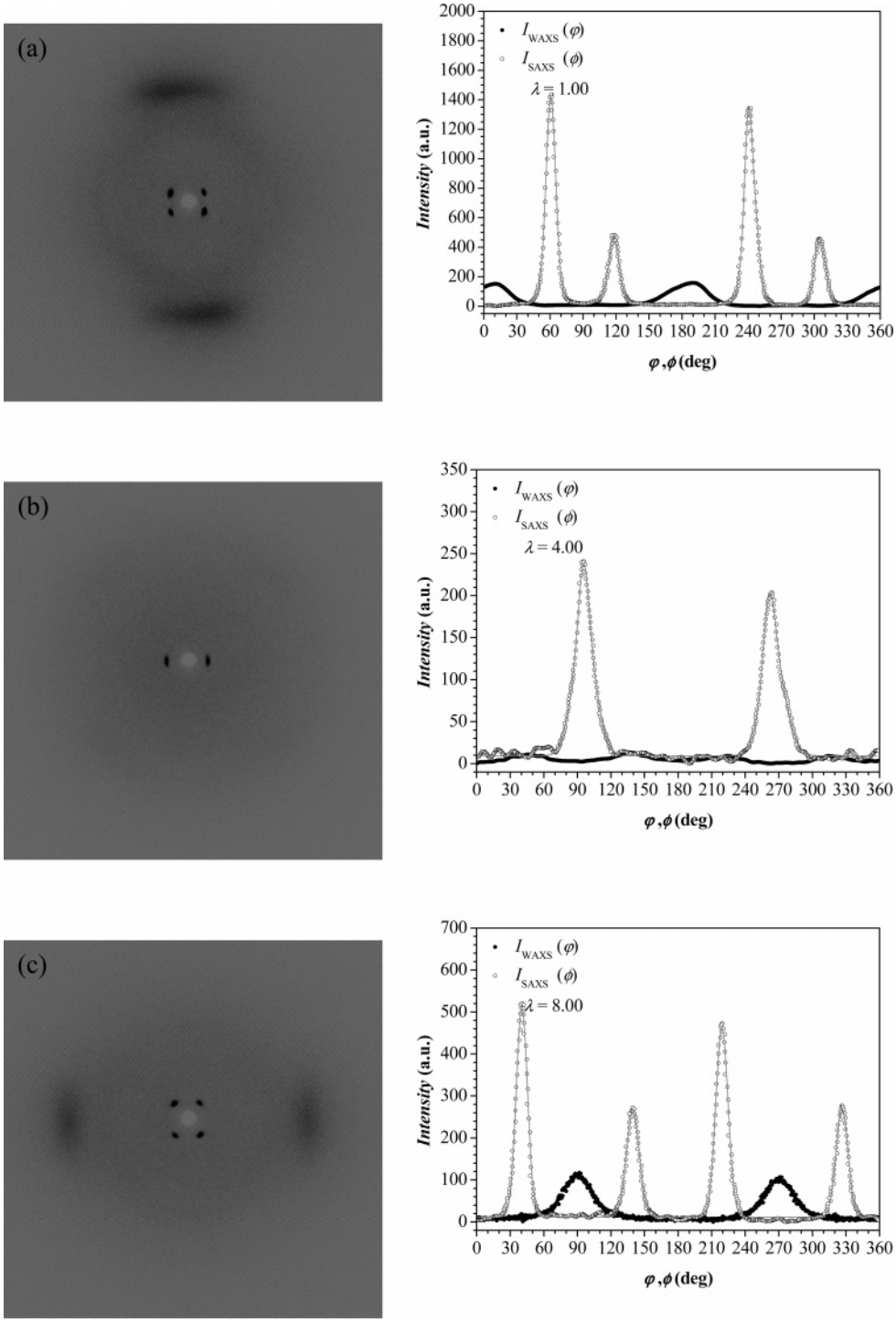

Figure 6. X-ray pictures of the MCEB7Azo2-2.5 sample at 25 °C in the SmC phase and WAXS and SAXS azimuthal intensity distributions at the uniaxial strain perpendicular to the director of (a) $\lambda = 1.00$, (b) $\lambda = 4.00$, and (c) $\lambda = 8.00$.

The thermoelastic behavior of this network reveals a shape memory effect as already investigated in detail by Rousseau.[28] While the change in length from the smectic into the isotropic phase is $\Delta l_{ISO} = 208\%$, on cooling, the unloaded sample only changes its length by $\Delta l_{ISO} = 11\%$. On cooling into the smectic phase the conical layer distribution structure does not reappear, but a polydomain becomes stable. However, on stretching this polydomain, the stable conical layer distribution structure reappears again.

Uniaxial Deformations

Uniaxial Stress−Strain Experiments. The main question is whether MCLCEs differ compared to SCLCEs on applying an external mechanical field parallel or perpendicular to the director and whether this force couples to the director and/or to the layer orientation.

In Figure 2, uniaxial stress−strain experiments are depicted, where deformations were performed parallel and perpendicular with respect to the director on the sample having the conical layer distribution structure.

Under deformation parallel to the director, two different linear regions can be observed. In the first region, for strain values of $1.00 < \lambda < 1.20$, the sample has a Young's modulus of $E_z = 1.3 \times 10^7$ N m^{-2}. In the second region, with strain values of $\lambda > 1.20$, the network shows a stiffer behavior with a Young's modulus of $E_z = 2.0 \times 10^7$ N m^{-2}. This deformation is a

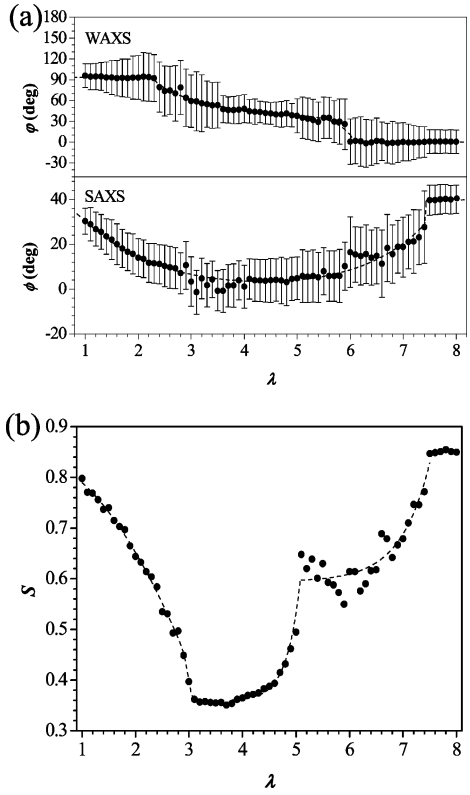

Figure 7. (a) Peak maxima in the WAXS (φ) and SAXS (ϕ) azimuthal intensity distributions as a function of uniaxial strain perpendicular to the director, λ. (b) Order parameter, S, as a function of uniaxial strain perpendicular to the director, λ.

reversible process, where the sample completely recovers its initial state on unloading.

In the deformation perpendicular to the director three regions can be differentiated: the first region with strain values of $1.00 < \lambda < 2.30$, the second at $2.30 < \lambda < 6.00$, and the third at $\lambda > 6.00$. The slopes of these three regions are $d\sigma_t/d\lambda = 3.0 \times 10^5$, 1.7×10^5, and 4.2×10^5 N m^{-2}, respectively. This deformation along the y-axis is a nonreversible process. The initial state can only be recovered by stretching the sample in the z-axis.

These stress−strain experiments already indicate that the mechanical response of these networks differ considerably from smectic-A side-chain elastomers. While parallel to the director in the z-direction the large modulus might be associated with the smectic layer compression modulus, no threshold stress or strain toward a low modulus could be identified. For smectic-A side-chain elastomers such a threshold indicates layer reorientation processes, which obviously do not occur in these networks. On the other hand, the large nonreversible deformation up to $\lambda \sim 9$ in the x,y-direction with respect to the parallel deformation indicates rearrangement of the structure that can be deduced from the low values of the slope.

Structure Elucidation. As expected, the mechanical property of this elastomer strongly depends on the direction of the applied force but differs considerably from that of smectic side-chain elastomers. To elucidate structural changes of the smectic structure of the elastomer, X-ray experiments were performed under deformation parallel and perpendicular to the director.

Uniaxial strain parallel to the director revealed two different moduli above and below a deformation of about 30%, which might indicate different deformation mechanisms. In Figure 3, the X-ray pictures at 25 °C are shown of the nonstretched sample (Figure 3a) and the sample stretched by 20% (Figure 3b). Additionally, the WAXS and SAXS azimuthal intensity distributions are given. The nonstretched sample exhibits four reflections in the small-angle region, indicating a tilt angle of the director with respect to the layer normal of 30°. The absolute intensities of these reflections differ, which implies a nonsymmetrical distribution of the layer normal about the director. As described below, this effect might be due to some shear deformations of the sample, e.g., because of nonsymmetrical clamping conditions. The two maxima of the azimuthal intensity distribution in the wide-angle region reveal a uniform director orientation and an order parameter of $S = 0.82$. In Figure 3b the results are shown for the elastomer strained by 20%. The most relevant change in the structure concerns the tilt angle ϕ, which increased from 31° to 40°, while the orientation of the director remains constant and parallel to the applied stress. Furthermore, the intensity distribution of the wide-angle reflections narrows indicating an increase of the order parameter from 0.82 to 0.89. Both results, i.e., the change of the tilt angle and the order parameter as a function of the deformation, are summarized in Figure 4. The order parameter, S, and the tilt angle, ϕ, increase with elongation and apparently remain constant for $\lambda > \sim 20\%$. This agrees with the stress−strain curve, where the modulus, E_z, changes from 1.3×10^7 N m^{-2} at $1.00 < \lambda < 1.20$ to 2.0×10^7 N m^{-2} for $\lambda > 1.20$. It is obvious that under these conditions director reorientation cannot occur, where the mechanical field is parallel to the director and where, due to the chemistry of the main-chain elastomers, the external field directly attacks the mesogenic units within the main chains. Therefore, a layer rotation, which is a component with threshold of stress or strain and low modulus, can be

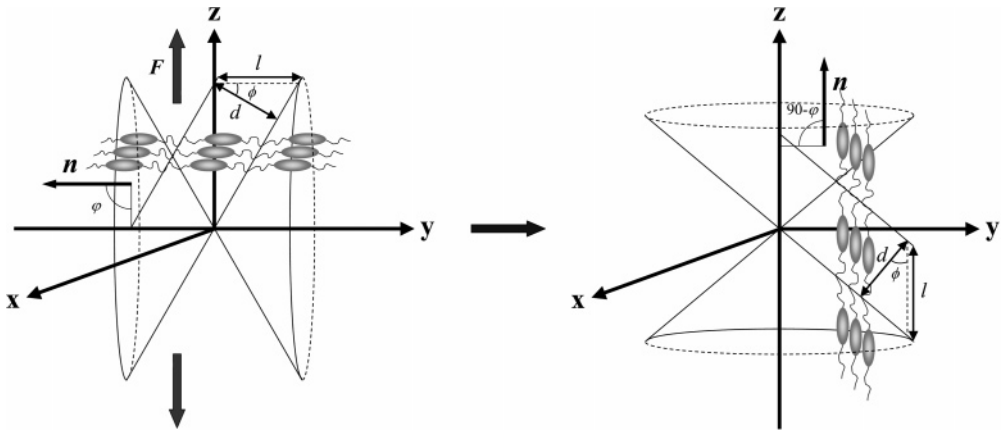

Figure 8. Uniaxial deformation process perpendicular to the director on a SmC MCLCE.

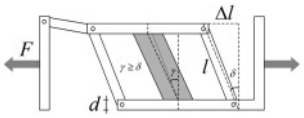

Figure 9. Setup for the shear experiments and geometrical relation between the applied angle δ and the shear strain γ.

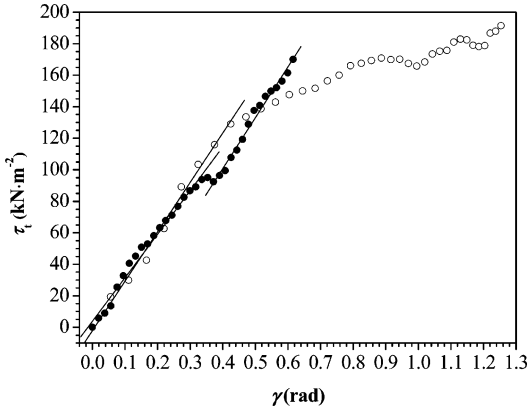

Figure 10. Shear stress−strain curves perpendicular (●) and parallel (○) to the director on a conical layer distribution structure of the elastomer MCEB7Azo2-2.5 at 25 °C in the SmC phase (τ_t = true shear stress).

excluded as observed for side-chain elastomers. For this system, however, the change of the tilt angle, which is equivalent to a layer rotation, might have the origin in an optimization of the packing of the mesogenic monomer units under strain. It has to be noted that a coupling between mechanical field and tilt angle has not been identified by experiments for side-chain elastomers so far. Recently, Stenull and Lubensky[29] predicted theoretically that such a rotation of the layer normal and the director may not occur simultaneously under shear. Such a shear deformation actually occurs locally in our sample (combined with a transverse compression) if one looks at an isolated uniform domain within the conical layer distribution structure. The increase of the order parameter suggests such rearrangement (Figure 5).

In Figure 4a, the angle φ (referred to Figure 1) differs slightly from 0° and denotes a difference between the direction of the external field and the director. As a consequence, some shear forces occur under deformation. The change of the intensities of the small-angle reflections from Figure 3a to 3b, which indicates a clear modification of the smectic layer distribution of the initial sample toward a uniformly aligned SmC structure, might be a consequence of such shear deformation. The shear experiments, described below, reinforce this assumption. The analysis of the intensity distribution of the small-angle reflections reveals a correlation length of the smectic structure of about $\xi = 40 \pm 1$ nm (16 ± 1 layers), which remains unchanged during the deformation process of the elastomer.

In the uniaxial stress perpendicular to the director, the mechanical measurement of the network already indicates a completely different response with a low slope value for the uniaxial strain perpendicular to the director and resembles the stress−strain behavior of SmA side-chain elastomers. For these SmA elastomers, the deformation perpendicular to the layer normal does not affect either the layer orientation or the director orientation and reflects the in-plane fluidity of the smectic phase structure.[2]

Starting from the nonstretched conical layer distribution structure (Figure 6a and Figure 8) with four reflections in the small-angle region and two in the wide-angle region, actually

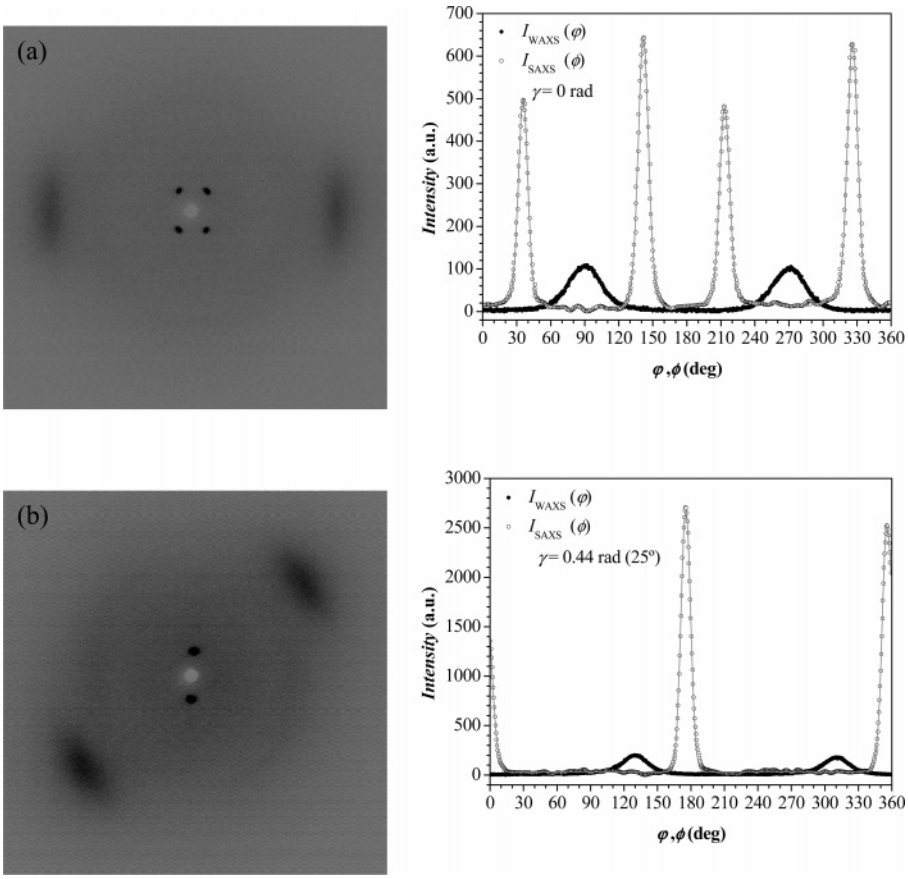

Figure 11. X-ray pictures of the MCEB7Azo2-2.5 sample at 25 °C in the SmC phase and WAXS and SAXS azimuthal intensity distributions at the shear strain perpendicular to the director of (a) $\gamma = 0$ rad and (b) $\gamma = 0.44$ rad.

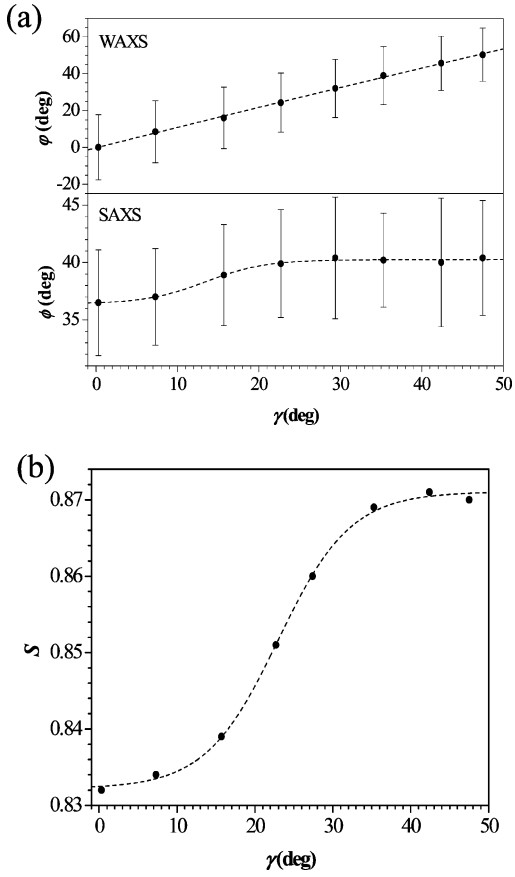

Figure 12. (a) Peak maxima in the WAXS (φ) and SAXS (ϕ) azimuthal intensity distributions as a function of shear strain perpendicular to the director, γ. (b) Order parameter, S, as a function of shear strain perpendicular to the director, γ.

a continuous layer rotation is observed toward an uniform orientation of the layer normal in the plane perpendicular to the applied stress (Figure 7a) at $\lambda = 2.30$. Obviously, the mechanical field couples to the smectic layers and removes defects of the initial conical layer distribution structure. The orientation of the layer normal in the plane perpendicular to the strain direction indicates that the uniaxial mechanical field is insufficient for a planar layer arrangement. A similar behavior is observed for nonordered (polydomain) SmA and lyotropic lamellar elastomers having an intrinsic oblate chain conformation. Only with a biaxial mechanical field does the layer normal become uniformly aligned in the direction perpendicular to the biaxial strain.[30,31] Consistent with this layer arrangement is the observation of four reflections in the wide-angle regime, which characterizes the tilt of the SmC phase. In contrast to the uniform director orientation of the initial conical layer distribution structure, the global director should have a conical distribution about the layer normal. Actually, the strong decrease of the order parameter from $S = 0.80$ to $S = 0.36$ (Figure 7b), where S reflects the product of the orientational and director order parameter, confirms such director configuration.

In the strain regime of $2.30 < \lambda < 6.00$, where the stress−strain curve is almost linear (Figure 2), a slight layer rotation of the layer normal occurs by 2° from 11° to about 9° passing through a minimum of 3° (Figure 7a). Most interestingly, the director simultaneously rotates by about 90° and indicates that the mechanical field causes an increase of the tilt angle. Above $\lambda > 6.00$, in the third regime, the director and layers become redistributed toward a conical layer distribution structure with a tilt angle of about 40°. In this strain regime, the mechanical field couples to the director and produces a structure as observed for the deformation process parallel to the director. This reorientation process is also reflected in the order parameter, which recovers the initial value of $S = 0.85$, as observed for the deformation process parallel to the director. The modulus, however, does not recover the modulus observed for the initial deformations parallel to the director. We have no explanation for this behavior, which resembles the stress−strain behavior of some nematic networks deformed perpendicular to the director. It has to be noted that such a reorientation process has not been observed for SmA and SmC elastomers so far. A reason might be that side-chain elastomers normally do not survive such large strains. The analysis of the intensity distribution of the small-angle reflections reveals a correlation length of the smectic structure of about $\xi = 39 \pm 2$ nm (16 ± 2 layers), which remains unchanged during the deformation process of the elastomer.

Shear Deformations

Shear Stress−Strain Experiments. Experiments on SmC side-chain elastomers with conical layer distribution structure already demonstrated that a shear field transforms a conical layer distribution structure into a monodomain possessing a uniform layer and director orientation.[8,9] The basic question is whether the SmC main-chain elastomers exhibit a similar behavior.

For the experiments, a self-constructed setup was used as shown in Figure 9, which allows the application of a shear force parallel and perpendicular to the director of the films. This setup can be used in a common stress−strain machine. A change in length, $\Delta l = l \sin \delta$, causes a shear angle γ of the sample by $\tan \gamma = l \sin \delta/(l \cos \delta - 2d)$. Note that under these experimental conditions no stress normal to the shear direction occurs. The shear stress τ was calculated for every shear angle γ. Furthermore, the shear modulus G was determined for each

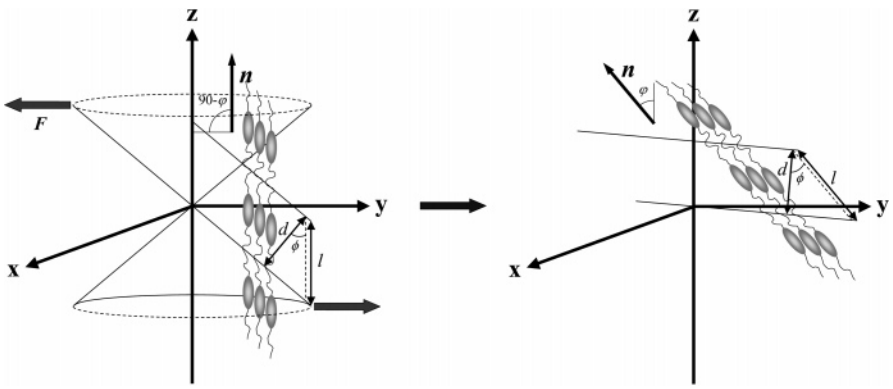

Figure 13. Shear deformation process perpendicular to the director on a SmC MCLCE.

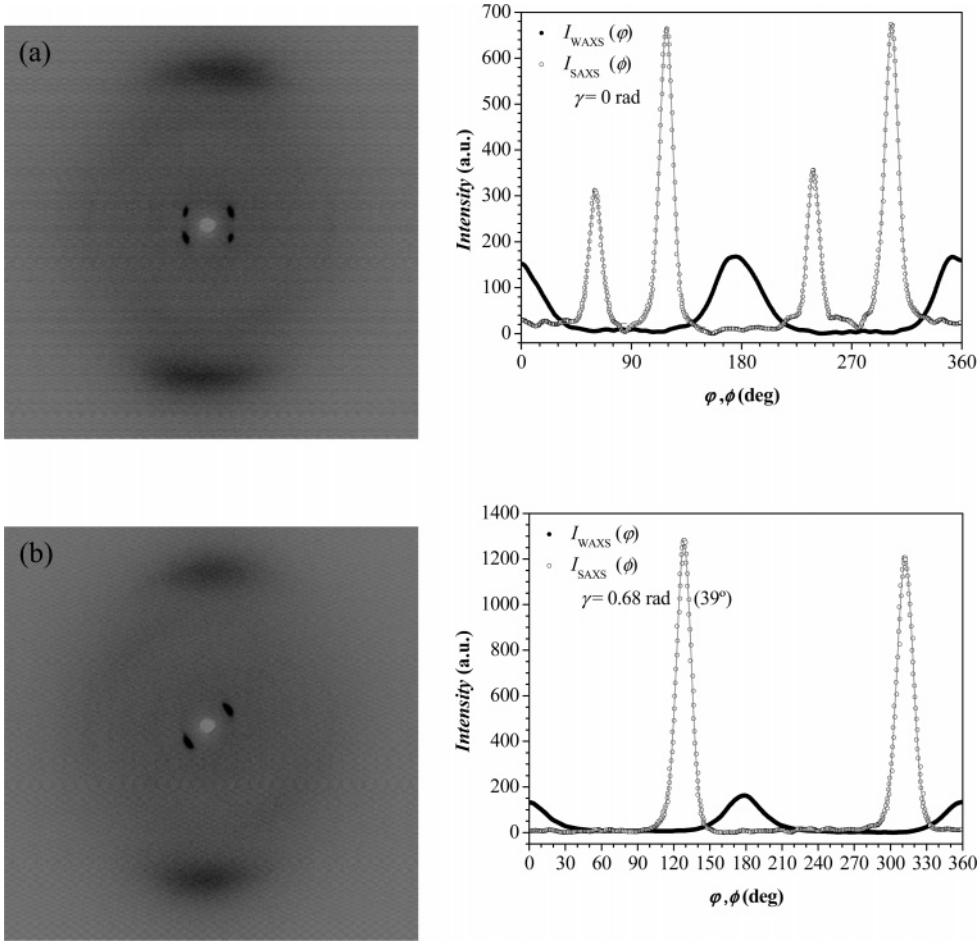

Figure 14. X-ray pictures of the MCEB7Azo2-2.5 sample at 25 °C in the SmC phase and WAXS and SAXS azimuthal intensity distributions at the shear strain parallel to the director of (a) $\gamma = 0$ rad and (b) $\gamma = 0.68$ rad.

shear deformation. To minimize friction of the joints, miniaturized ball bearings are employed. Test measurements without an elastomer reveal no contribution of friction within the experimental accuracy.

In Figure 10, where the shear stress τ is plotted vs the shear angle γ, the results are presented for the shear deformation parallel and perpendicular to the director of the network with conical layer distribution structure. Interestingly for both deformation modes, at the beginning of the shear deformation ($\gamma < 21°$; 0.37 rad) the same modulus of $G \sim 3.2 \times 10^5$ N m^{-2} was found. This might indicate that both shear geometries cause the same reorientation process. For the shear deformation perpendicular to the initial director orientation above this angle, a local soft response occurs in the regime between 19° (0.34 rad) $< \gamma <$ 21° (0.37 rad). Above this angle again a linear response of the shear stress τ occurs with about the same modulus. For the shear deformation parallel to the initial director orientation above $\gamma >$ 24° (0.42 rad) the film wrinkles upon further shear deformation, and the deformation process becomes irreversible. The elastomer does not recover its original shape on unloading.

Structure Elucidation. Starting from the initial sample with the conical layer distribution structure (Figure 11a), the shear stress perpendicular to the director couples to the director as well as to the layer orientation and causes a continuous rotation of the director and the layers with the shear angle. This process, however, preferentially affects those layers, where the smectic layer normal can rotate toward the shear force. It minimizes the angle between the direction of shear force and the angle within the layer plane directing toward the shear force. The same

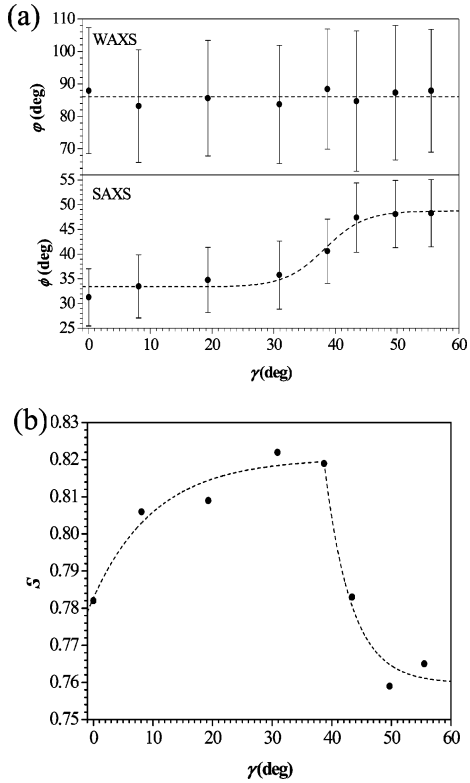

Figure 15. (a) Peak maxima in the WAXS (φ) and SAXS (ϕ) azimuthal intensity distributions as a function of shear strain parallel to the director, γ. (b) Order parameter, S, as a function of shear strain parallel to the director, γ.

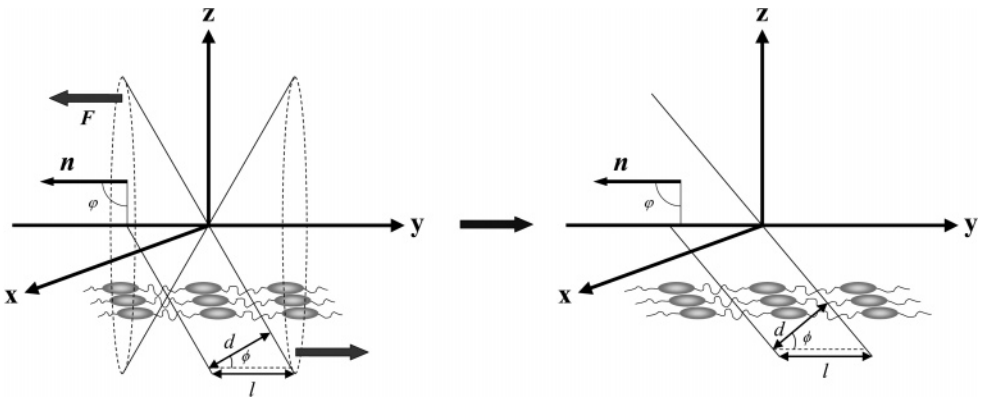

Figure 16. Shear deformation process parallel to the director on a SmC MCLCE.

obviously holds for the director reorientation. At about $\gamma \sim 25°$, which corresponds to the dip in the shear stress−strain curve, all layers are completely removed that are not aligned in the shear direction (Figure 11b).

Additionally it has to be noted that this reorientation process directly affects the intrinsic tilt angle, which increases continuously from 37° to 41° and remains unaffected at larger shear strain (Figure 12a). It resembles the uniaxial strain behavior of the elastomer parallel to the director, which also increases the tilt up to a constant angle. Above the shear deformation of $\gamma \sim 25°$, the layers as well as director rotate simultaneously with the shear angle. An increase of the order parameter indicates a growing perfection of the structure toward a SmC monodomain (Figure 13). The analysis of the line shape of the SAXS reflections yields a correlation length of about $\xi = 40 \pm 2$ nm (16 ± 1 layers), which remains unchanged during the deformation process of the sample.

Applying the shear deformation parallel to the director also causes a reorientation leading to a monodomain structure (Figure 14). This deformation process, however, basically differs from the previous experiment. The shear strain does not affect the director orientation, which remains fixed parallel to the shear direction (Figure 16). Only those layers become reoriented, where the angle between layer plane and shear angle increases with shear. The question remains as to whether this process also modifies the orientation of layers of the conical layer distribution structure, where the layer plane is already oriented within the shear plane.

If we compare the ratio between the intensities of the WAXS and SAXS (Figure 14b) with that of the reoriented sample from the previous experiment (Figure 11b), the reorientation for the shear process parallel to the director is less efficient. The intensity ratio, I_{SAXS}/I_{WAXS}, for the sample ordered by the shear process perpendicular to the director is 14 while it is 7 for the sample sheared parallel to the director. Obviously, the layers that are oriented with their layer plane within the shear plane are not influenced by the shear process. Detailed X-ray investigations have to clarify this problem. An indication that this orientation process leading to a monodomain is less efficient might also be indicated by the order parameter, which only increases to $S \sim 0.82$ for the shear angle of $\gamma \sim 40°$ (Figure 15b), in contrast to $S \sim 0.87$ (Figure 12b) for the previous experiment. Above a deformation of $\gamma \sim 25°$ the shear process becomes irreversible, and the ordered structure is destroyed for $\gamma > 40°$ by rotation of the director and the layers. The analysis of the line shape of the SAXS reflections yields a correlation length of about $\xi = 47 \pm 2$ nm (19 ± 1 layers), which remains unchanged during the deformation process of the sample.

Conclusion

Different deformation processes have been studied and analyzed on a conical layer distribution structure of SmC main-chain liquid-crystalline elastomer. Stress−strain and X-ray experiments were applied to identify structural modifications during deformation.

The uniaxial deformation of the elastomer parallel to the director causes an increase of the tilt angle without affecting the director orientation, which is accompanied by an increase of the Young modulus parallel to the director. Uniaxial deformation perpendicular to the director produces a reorientation of the director parallel to the applied force. This reorientation process also affects the tilt angle of the smectic structure. After complete reorientation a tilt angle is observed that corresponds to the tilt angle of the sample under uniaxial strain parallel to the director.

The shear deformation perpendicular to the director is a reversible process and couples to the layer as well as to the director orientation. A highly ordered monodomain is obtained by this reversible reorientation process. The shear deformation parallel to the director only affects the layer reorientation toward a monodomain while the director orientation remains unchanged. This irreversible process, however, does not produce a highly ordered monodomain.

The basic difference between main- and side-chain elastomers is that in main-chain elastomers the mechanical field always couples to the tilt angle of the SmC phase structure. This opens new interesting aspects especially for chiral SmC* elastomers, where the tilt angle determines the optical and ferro-electrical properties. Further experiments have to be carried out to investigate these properties as a function of mechanical field.

Experimental Part

X-ray Diffraction Experiments (XRD). X-ray scattering experiments were performed using a Philips PW 1730 rotating anode (4 kW) in order to obtain direct information on the SAXS and WAXS reflections in the smectic-C phases. Cu Kα radiation (1.5418 Å) filtered by a graphite monochromator and collimated by a 0.8 mm collimator was used. The incident beam was normal to the surface of the film. The scattered X-ray intensity was detected by a Schneider image plate system (700 × 700 pixels, 250 μm resolution). Samples were placed in a self-constructed holder where temperature was controlled by a Haake-F3 thermostat. From the SAXS intensities the layer distance (d) (Lorentzian distribution), the layer angle (ϕ) (Gaussian distribution), and the correlation length (ξ) (pseudo-Voigt distribution) were calculated. From the WAXS intensities, the mesogen distance was calculated using a Lorentzian distribution, the mesogen angle (φ) (Gaussian distribution), and the order parameter ($S = S_d S_N$) according to Lovell and Mitchell,[32,33]

where S_d is the director order parameter and S_N the order parameter that refers to the local orientational order parameter. For samples having a macroscopically uniform alignment of the director we assume that $S_d \approx 1$. All error bars are calculated as a half of the fwhm from the intensity Gaussian distribution of the ϕ and φ.

Uniaxial and Shear X-ray Diffraction Experiments. Uniaxial and shear deformations were carried out using a uniaxial stress−strain self-constructed apparatus and a shear stress−strain apparatus. All measurements were done at 25 °C and 1 h of relaxation time after each stretching or shearing step.

Uniaxial and Shear Stress−Strain Experiments. Stress−strain measurements were performed with a self-constructed apparatus. In a cell controlled by a Haake-F6 thermostat and equipped with a Pt100 thermoresistor, the sample was stretched by one Owis SM400 microstep motor and controlled by an Owis SMK01 microstep controller. The stress (σ) was measured by a HBM PW4FC3 transducer load cell (300 g) and analyzed by an HBM KW3073 high-performance strain gage indicator. All relevant data such as temperature, uniaxial strain ($\lambda = L/L_0$), shear strain (γ), uniaxial stress (σ), and shear stress (τ) were continuously logged. A personal computer controlled the deformation stepwise as specified by a script file. After each deformation step, the static responses to the deformation, the uniaxial stress (σ), or shear stress (τ) were recorded once equilibrium was reached according to the slope and the standard deviation of the continuously logged data. In the case of shear stress−strain measurements, a shear stress−strain apparatus was attached to the arm connected to the load cell.

Synthesis of 4-Hydroxyphenyl 4-Hydroxybenzoate (HPHB). In a 1 L round-bottomed flask equipped with stirrer, condenser, temperature probe, and nitrogen sweep, 62.7 g (0.5 mol) of 4-hydroxybenzoic acid and 500.0 g (4.5 mol) of hydroquinone were placed. The mixture was heated at 260 °C for 2 h, after which the reaction mixture was poured into 2.5 L of water. The white solid was recrystallized from (1:1 v/v) ethanol/water. Yield: 56.5 g (54%). ^{1}H NMR (300 MHz, DMSO-d_6): δ = 8.03 (2H, d, *o*-Ar, J = 8.5 Hz), 7.95 (2H, s, ArOH), 7.23 (2H, d, *o*-Ar′, J = 8.9 Hz), 7.07 (2H, d, *m*-Ar′, J = 8.9 Hz), 6.93 (2H, d, *m*-Ar, J = 8.5 Hz) ppm. ^{13}C NMR (75 MHz, DMSO-d_6): δ = 165.0 (COOAr), 164.1 (ArOH), 155.8 (Ar′OH), 145.3 (Ar′OCO), 134.0 (2C, *o*-ArH), 123.7 (2C, *o*-Ar′H), 118.9 (ArCOO), 118.6 (2C, *m*-Ar′H), 115.9 ppm (2C, *m*-Ar′H). FTIR (NaCl): 3267 (st, O−H), 1689 (st, C═O), 1446 (δ, OH), 1286 (st, C−O), 1234 cm^{-1} (st as, C−O); mp: 245 °C.

Synthesis of 4-[4-(Vinyloxy)butoxy]phenyl 4-[4-(Vinyloxy)-butoxy]benzoate (GB7). In a 250 mL round-bottomed flask, 5.0 g (22 mmol) of 4-hydroxyphenyl 4-hydroxybenzoate (HPHB) and 12.5 g (48 mmol) of triphenylphosphine (PPh_3) were placed, and 100 mL of anhydrous THF was added. The system was magnetically stirred and purged with nitrogen for 15 min, after which 5.0 g (43 mmol) of 4-(vinyloxy)butan-1-ol was added. In the next step, the solution was magnetically stirred under nitrogen, and 9.7 g (48 mmol) of diisopropyl aza-1,2-dicarboxylate (DiPAD) was added. The reaction was stirred at room temperature and controlled by TLC (SiO_2, CH_2Cl_2). Completion of the reaction was coupled with the disappearance of the starting phenol derivative (8 h). Then hexane/AcOEt (5:1 v/v) was added, and a white solid, triphenylphosphine oxide, was precipitated. The solution was filtered and evaporated. The residue was purified by column chromatography using CH_2Cl_2 as the eluent to yield the product (8.8 g, 95%). ^{1}H NMR (300 MHz, $CDCl_3$): δ = 8.13 (2H, d, *o*-Ar, J = 9.0 Hz), 7.10 (2H, d, *o*-Ar′, J = 9.2 Hz), 6.96 (2H, d, *m*-Ar′, J = 9.0 Hz), 6.92 (2H, d, *m*-Ar, J = 9.0 Hz), 6.49 (2H, dd, C*H*═CH_2, J = 14.4 Hz, J = 6.7 Hz), 4.20 (2H, dd, *cis*-CH═CH_2, J = 14.4 Hz, J = 1.9 Hz), 4.09 (2H, t, CH_2OAr, J = 6.0 Hz), 4.00 (2H, dd, *trans*-CH═CH_2, J = 6.7 Hz, J = 1.9 Hz), 4.00 (2H, t, CH_2OAr′, J = 6.0 Hz), 3.77 (2H, t, CH_2, J = 5.9 Hz), 3.76 (2H, t, CH_2, J = 5.9 Hz), 2.02−1.79 ppm (8H, m, CH_2). ^{13}C NMR (75 MHz, $CDCl_3$): δ = 165.2 (COOAr), 163.2 (ArOCH_2), 156.6 (Ar′OCH_2), 151.8 (2C, *C*H═CH_2), 144.4 (Ar′OCO), 132.2 (2C, *o*-ArH), 122.5 (2C, *o*-Ar′H), 121.8 (ArCOO), 115.0 (2C, *m*-Ar′H), 114.2 (2C, *m*-ArH), 86.5 (CH═*C*H_2), 86.4 (CH═*C*H_2), 67.8 (CH_2OAr), 67.7 (CH_2OAr′), 67.5 (*C*H_2OCH═CH_2), 67.4 (*C*H_2OCH═CH_2), 25.9 (CH_2), 25.8 (CH_2), 25.7 (CH_2), 25.6 ppm (CH_2). FTIR (NaCl): 1725 (st, C═O), 1612 (st, C═C), 1292 (st, C−O), 1253 cm^{-1} (st, C−O); mp: C 72 SmC 87 I °C.

Synthesis of (*E*)-4-Hydroxy-4′-methoxyzobenzene (MHAB). In a 50 mL round-bottomed flask, 1.0 g (8 mmol) of 4-methoxyaniline was placed, and 10 mL of water and 5 mL of 37% HCl solution and some crushed ice were added. This solution was cooled at 0 °C with an external ice−water bath. Then 616 mg (9 mmol) of $NaNO_2$ in 5 mL of water was added at 0−5 °C, and the reaction mixture was left for 15 min, during which 4-methoxybenzenediazonium chloride was formed. In the next step, in a 100 mL flask, 764 mg (8 mmol) of phenol and 2.7 g of NaOH were placed, and 10 mL of water was added. This solution was kept below 5 °C. The first solution of the diazonium salt was then dropped slowly into the reaction mixture, and the appearance of a red compound was observed. After 30 min the azobenzene derivative was precipitated using 2 M HCl solution. The precipitate was filtered, washed several times with water, and dried, and the residue was purified by column chromatography using CH_2Cl_2 as the eluent to yield the product (1.8 g, 95%). ^{1}H NMR (300 MHz, $CDCl_3$): δ = 7.88 (2H, d, *o*-Ar, J = 9.5 Hz), 7.82 (2H, d, *m*-Ar′, J = 8.8 Hz), 7.00 (2H, d, *m*-Ar′, J = 8.8 Hz), 6.92 (2H, d, *o*-Ar, J = 9.5 Hz), 5.44 (1H, s, ArOH), 3.89 ppm (3H, s, CH_3O). ^{13}C NMR (75 MHz, $CDCl_3$): δ = 161.5 (Ar′OCH_3), 157.6 (ArOH), 147.1 (Ar′N═N), 146.9 (ArN═N), 124.5 (*o*-ArH), 124.3 (*o*-Ar′H), 115.7 (*m*-ArH), 114.1 (*m*-Ar′H), 55.6 ppm (CH_3O). FTIR (NaCl): 3625 (st, O−H), 1495 (st, N═N), 1238 cm^{-1} (st, C−O); mp: 142 °C.

Synthesis of (*E*)-4,4′-Dihydroxyazobenzene (DHAB). In a 100 mL round-bottomed flask, 1.0 g (4 mmol) of (*E*)-4-hydroxy-4′-methoxyzobenzene (MHAB) was placed under nitrogen at −78 °C, and 17.5 mL of 1 M BBr_3 solution in CH_2Cl_2 was added slowly. After the addition, the mixture was left to warm to room temperature and controlled by TLC (SiO_2, AcOEt/hexane, 1:1). After 2 h the mixture was cooled at 0 °C, and 2 M NaOH solution was added. Then 2 M HCl was added until the reaction mixture reached a pH = 1 and was then extracted with AcOEt. The solution was filtered and evaporated. The residue was purified by column chromatography using a mixture of AcOEt/hexane (1:1 v/v) as eluent to yield the product (0.9 g, 92%). ^{1}H NMR (300 MHz, DMSO-d_6): δ = 10.10 (2H, s, ArOH), 7.71 (4H, d, *o*-Ar, J = 8.8 Hz), 6.90 ppm (4H, d, *m*-Ar, J = 8.6 Hz). ^{13}C NMR (75 MHz, DMSO-d_6): δ = 160.1 (2C, ArOH), 145.6 (2C, ArN═N), 124.3 (4C, *o*-ArH), 115.9 ppm (4C, *m*-ArH). FTIR (NaCl): 3598 (st, O−H), 1492 cm^{-1} (st, N═N); mp: 218 °C.

Synthesis of (*E*)-4,4′-Bis(hex-5-en-1-yloxy)azobenzene (AZO). In a 50 mL two-necked round-bottomed flask, 200 mg (0.093 mmol) of (*E*)-4,4′-dihydroxyazobenzene (DHAB) and 7.8 mg (0.20 mmol) of NaH (60% dispersion in mineral oil) were weighed. A reflux condenser was then attached, and the system was purged with nitrogen for about 20 min, after which 10 mL of anhydrous DMF was added. The solution was magnetically stirred and heated to 80 °C; 30 mg (0.19 mmol) of 6-bromo-1-hexen dissolved in 2 mL of anhydrous DMF was added. After 16 h the reaction was cooled to room temperature and diluted with 50 mL of CH_2Cl_2 and 50 mL of H_2O and extracted with CH_2Cl_2. The organic layer was dried over anhydrous sodium sulfate, filtered, and evaporated. The crude product was purified by column chromatography using a mixture of CH_2Cl_2/hexane (4:6 v/v) as eluent to yield the product (340 mg, 97%). ^{1}H NMR (300 MHz, $CDCl_3$): δ = 7.87 (4H, d, *o*-Ar, J = 9.0 Hz), 6.99 (4H, d, *m*-Ar, J = 9.0 Hz), 5.85 (2H, ddt, C*H*═CH_2, J = 16.9 Hz, J = 10.4 Hz, J = 6.7 Hz), 5.06 (2H, ddt, *cis*-CH═CH_2, J = 17.3 Hz, J = 2.0 Hz, J = 1.6 Hz), 5.00 (2H, ddt, *trans*-CH═CH_2, J = 10.2 Hz, J = 2.0 Hz, J = 1.0 Hz), 4.04 (4H, t, CH_2O, J = 6.3 Hz), 2.15 (4H, tdt, CH_2, J = 7.3 Hz, J = 6.9 Hz, J = 1.2 Hz), 1.84 (4H, tt, CH_2, J = 6.9 Hz, J = 6.5 Hz) 1.60 ppm (4H, tt, CH_2, J = 7.1 Hz, J = 6.7 Hz). ^{13}C NMR (75 MHz, $CDCl_3$): δ = 161.1 (2C, ArOCH_2), 147.0 (2C, ArN═N), 138.4 (2C, *C*H═CH_2), 124.3 (4C, *o*-ArH), 114.8 (2C, CH═*C*H_2), 114.6 (4C, *m*-ArH), 68.0 (2C, CH_2O), 33.4 (2C, CH_2), 28.6 (2C, CH_2), 25.3 ppm (2C, CH_2). FTIR (NaCl): 1603 (st, C═CH_2), 1498 (st, N═N), 1250 (st, C−O), 910 cm^{-1} (δ oop, CH═CH_2). UV (EtOH,

25 °C): $\lambda_{max} = 356$, 436 nm ($\epsilon = 25\,000$, 3000 L mol^{-1} cm^{-1}); mp: C_1 74 C_2 97 I °C.

Synthesis of MCEB7Azo2-2.5. In a 5 mL flask were placed main-chain mesogen 4-[4-(vinyloxy)butoxy]phenyl 4-[4-(vinyloxy)-butoxy]benzoate, GB7 (324 mg, 0.76 mmol), (*E*)-4,4′-bis(hex-5-en-1-yloxy)azobenzene, AZO (15 mg, 0.04 mmol), 2,4,6,8,10-pentamethyl-1,3,5,7,9,2,4,6,8,10-pentaoxapentasilecane, PMPOPS (6 mg, 0.02 mmol), and 1,1,3,3-tetramethyldisiloxane, TMDSO (101 mg, 0.75 mmol), and 1.5 mL of thiophene-free toluene and 60 μL of 1% Pt cyclooctadieneplatinum(II) chloride, Pt(COD)Cl_2, in dichloromethane were added. The mixture was placed in the spinning Teflon cell form which was heated at 60 °C for 4 h at 5000 rpm. Afterward, the reactor was cooled and the elastomer was removed from the wall. Some loads were applied in order to align the sample during the deswelling process. In this first step the elastomer is not totally cross-linked. In order to fix this orientation, the cross-linking reaction was completed by leaving the elastomer in the oven under vacuum at 60 °C for 2 days. In order to measure the soluble content (5.7%) of the samples, each elastomer was placed in a liquid−solid extractor for 1 day, using hexane as the solvent.

Acknowledgment. The authors acknowledge financial support from the Research Training Networks FUNCTIONAL LIQUID-CRYSTALLINE ELASTOMERS (FULCE-HPRN-CT-2002-00169) and Fonds der Chemischen Industrie.

References and Notes

(1) Nishikawa, E.; Finkelmann, H. *Macromol. Chem. Phys.* **1999**, *200*, 312.
(2) Nishikawa, E.; Finkelmann, H.; Brand, H. R. *Macromol. Rapid Commun.* **1997**, *18*, 65.
(3) Nishikawa, E.; Finkelmann, H. *Macromol. Chem. Phys.* **1997**, *198*, 1531.
(4) Stannarius, R.; Kohler, R.; Dietrich, U.; Losche, M.; Tolksdorf, C.; Zentel, R. *Phys. Rev. E* **2002**, *65*, 041707.
(5) Stannarius, R.; Kohler, R.; Roessle, M.; Zentel, R. *Liq. Cryst.* **2004**, *31*, 895.
(6) Komp, A.; Finkelmann, H. *Macromol. Rapid Commun.* **2007**, *28*, 55.
(7) Hiraoka, K.; Sagano, W.; Nose, T.; Finkelmann, H. *Macromolecules* **2005**, *38*, 7352.
(8) Hiraoka, K.; Finkelmann, H. *Macromol. Rapid Commun.* **2001**, *22*, 456.
(9) Hiraoka, K.; Stein, P.; Finkelmann, H. *Macromol. Chem. Phys.* **2004**, *205*, 48.
(10) Semmler, K.; Finkelmann, H. *Macromol. Chem. Phys.* **1995**, *196*, 3197.
(11) Benne, I.; Semmler, K.; Finkelmann, H. *Macromol. Rapid Commun.* **1994**, *15*, 295.
(12) Adams, J. M.; Warner, M. *Phys. Rev. E* **2005**, *72*, 011703.
(13) Adams, J. M.; Warner, M. *Phys. Rev. E* **2006**, *73*, 031706.
(14) Lubensky, T. C.; Terentjev, E. M.; Warner, M. *J. Phys. II* **1994**, *4*, 1457.
(15) Adams, J. M.; Warner, M. *Phys. Rev. E* **2005**, *71*, 021708.
(16) Terentjev, E. M.; Warner, M.; Lubensky, T. C. *Europhys. Lett.* **1995**, *30*, 343.
(17) Weilepp, J.; Brand, H. R. *Macromol. Theory Simul.* **1998**, *7*, 91.
(18) Stenull, O.; Lubensky, T. C. *Phys. Rev. Lett.* **2005**, *94*, 018304.
(19) Stenull, O.; Lubensky, T. C. *Phys. Rev. E* **2006**, *73*, 030701.
(20) Donnio, B.; Wermter, W.; Finkelmann, H. *Macromolecules* **2000**, *33*, 7724.
(21) Giamberini, M.; Amendola, E.; Carfagna, C. *Mol. Cryst. Liq. Cryst. Sci. Technol., Sect. A* **1995**, *266*, 9.
(22) Mitsunobu, O.; Wada, M.; Sano, T. *J. Am. Chem. Soc.* **1972**, *94*, 679.
(23) Junge, D. M.; McGrath, D. V. *Chem. Commun.* **1997**, *9*, 857.
(24) Furniss, B. S.; Hannaford, A. J.; Smith, P. W. G.; Tatchell, A. R. In *Vogel's Textbook of Practical Organic Chemistry*, 5th ed.; Longman: Harlow, UK, 1989; p 946.
(25) Amaike, M.; Kobayashi, H.; Sakurai, K.; Shinkai, S. *Supramol. Chem.* **2002**, *14*, 245.
(26) Imai, Y.; Naka, K.; Chujo, Y. *Macromolecules* **1999**, *32*, 1013.
(27) Ishizaki, M.; Yamada, M.; Watanabe, S. I.; Hoshino, O.; Nishitani, K.; Hayashida, M.; Tanaka, A.; Hara, H. *Tetrahedron* **2004**, *60*, 7973.
(28) Rousseau, I. A.; Mather, P. T. *J. Am. Chem. Soc.* **2003**, *125*, 15300.
(29) Stenull, O.; Lubensky, T. C. *Phys. Rev. E* **2007**, *76*, 011706.
(30) Fischer, P.; Schmidt, C.; Finkelmann, H. *Macromol. Rapid Commun.* **1995**, *16*, 435.
(31) Nishikawa, E.; Yamamoto, J.; Yokoyama, H.; Finkelmann, H. *Macromol. Rapid Commun.* **2004**, *25*, 611.
(32) Lovell, R.; Mitchell, G. R. *Acta Crystallogr. A* **1981**, *37*, 135.
(33) Mitchell, G. R.; Windle, A. H. In *Developement in Crystalline Polymers-2*; Basset, D. C., Ed.; Elsevier Applied Science: London, 1988; Vol. 3, p 115.

MA7025644